Journal of Thermal Analysis and Calorimetry
https://doi.org/10.1007/s10973-020-10013-5

Influence of the adjacent layers on the crystallization kinetics of $Ge_2Sb_2Te_5$ thin films

Alexey Yakubov[1] · Alexey Sherchenkov[1] · Alexey Babich[1] · Petr Lazarenko[1] · Irina Sagunova[1] · Elena Kirilenko[2]

Received: 20 August 2019 / Accepted: 29 June 2020
© Akadémiai Kiadó, Budapest, Hungary 2020

Abstract

The influence of the adjacent layers (SiO_2, Al, Ni, Ti, W, TiN, TiN/W) on the crystallization kinetics of $Ge_2Sb_2Te_5$ thin films was investigated using the techniques based on the application of two different methods—differential scanning calorimetry and measurements of the resistivity temperature dependences. Thin films were deposited by the magnetron sputtering. The composition of the films was determined by the Auger spectroscopy and was close to $Ge_2Sb_2Te_5$. X-ray diffraction was used to investigate the structure of thin films and showed that the as-deposited films were in an amorphous state, while heat treatment at 250 °C for 30 min led to the crystallization to the cubic (rock salt) phase. Effective activation energy of crystallization obtained by differential scanning calorimetry at the beginning of the crystallization was 1.8 eV and then slightly decreased to 1.7 eV at the end of the process. The values of the effective activation energy obtained from the measurements of the resistivity temperature dependences were in the range of 2.5–2.9 eV at the beginning and in the range of 2.2–3.5 eV at the end of the crystallization process. The difference in the effective activation energies of crystallization for the GST225 thin films deposited on the different sublayers is caused by the influence of the neighboring sublayers on the crystallization process. It was found that crystallization temperatures correlate with the effective activation energies and increase with their growth.

Keywords Phase-change memory · $Ge_2Sb_2Te_5$ · Kinetics of crystallization

Introduction

Currently, the phase-change memory (PCMe) is considered to be one of the promising candidates for the next generation of nonvolatile memory devices due to the high operation speed, low power consumption, high endurance, extended scalability and compatibility with CMOS technology [1–3]. Recent investigations are directed on the development of the PCMe with the multi-level cells, which allows to store the multiple bits in the memory cell and is powerful method to increase the data density and reduce the cost per bit [4–7].

Compositions in ternary system Ge–Sb–Te (GST) are widely studied as active layers for PCMe devices, in particular $Ge_2Sb_2Te_5$ (GST225), due to the high stability at room temperatures and fast crystallization rate [3, 8, 9].

✉ Alexey Yakubov
alexsey007@mail.ru

[1] National Research University of Electronic Technology, Bld. 1, Shokin Square, Zelenograd, Moscow, Russia 124498

[2] Nanotechnology Institute of Microelectronics of RAS, Bld. 16A/11, Nagatinskaya street, Moscow, Russia 115487

The working principle of such memory is based on the reversible phase transition between the crystalline state with low resistivity and amorphous state with high resistivity. Both states are stable, so they can be used to store binary information [10]. The switching between the two states occurs by means of local temperature increase due to the electrical or laser impulses. In this case, the ability to control the fraction of amorphous and crystalline phases of the active PCMe material during the crystallization by controlling parameters of the programmable pulse will allow to write several nonvolatile reliable and repeatable levels and so create multi-level cell. For example, 4-bit cell was presented in [11]. So, the operation rate of the memory devices is determined by the reversible amorphous to crystalline transitions. However, the transition from crystalline to amorphous state (reset operation) is sufficiently at least on the order of magnitude faster than the opposite transition from amorphous to crystalline state (set operation) [3]. Thus, exactly crystallization kinetics determines the operation rate of the phase-change memory devices. Therefore, investigation of the kinetics and mechanisms of crystallization has not only strong theoretical but also practical motivation for

Published online: 13 July 2020

the development of the high-speed phase-change memory technology. In particular, it is important for the creation of the multi-level PCMe cells, when it is necessary to stop precisely crystallization process and fix intermediate crystallization states of the active phase-change memory material layer [12–14].

Several methods were used for the investigation of the kinetics and mechanisms of the crystallization process in the materials and thin films on their basis: differential scanning calorimetry (DSC) [15–23], X-ray diffraction (XRD) [24], transmission electron microscopy (TEM) [25–28], optical reflectance/transmittance [29–35] and electrical resistance [36–48]. Determined effective activation energies of crystallization for Ge–Sb–Te materials appear in the wide range from 0.81 to 4.3 eV, though most results lay in the range from 2.0 to 3.0 eV. Such discrepancy can be explained by the difference in the fabrication methods and measuring techniques.

All investigations were carried out in non-isothermal and isothermal conditions. However, the use of non-isothermal measurements allows to overcome a major problem of the isothermal experiments, which is connected with the loss of the data at the beginning of heating due to the requirement of some time to reach the necessary temperature [49]. However, a typical solid state process has a maximum reaction rate at the beginning of the transformation. In the case of non-isothermal experiments, this problem is absent. In most cases, only average effective activation energies of crystallization were determined using the Kissinger method. However, effective activation energy can vary significantly during the crystallization depending on the fraction of the crystallized material (conversion) and variation of the mechanism, which change kinetics of the process. In addition, the knowledge of only effective activation energy does not allow to estimate crystallization time and so determinate possible data processing and storage times of PCMe cells. For this purpose, it is necessary to determine kinetic triplet (effective activation energy, pre-exponential factor and reaction model) for the crystallization process of the PCMe thin films.

Differential scanning calorimetry is a direct method of studying processes accompanied by the heat effects and is actively used for the investigation of the kinetics and mechanisms of the crystallization. In this case, samples are usually prepared by scraping the film from the substrate and pressing the powder in the crucible. This is far from the real situation in the PCMe cell with monolithic GST film, crystallization of which can be influenced by the neighbor layers.

It should be noted that the crystallization process of the PCMe material layers is significantly influenced by the neighbor dielectric thin films [25, 27, 29, 30, 36, 40]. Such configuration is typical for the optical PCMe, where active recording layer is sandwiched between the dielectric materials [50], which are used as transparent protective capping layers to prevent vaporization of the phase-change material during the recording process by laser irradiation. In the case of electrical PCMe, the neighbor layers to the active recording layer are conducting electrode. However, the influence of such conducting layers on the kinetics and mechanisms of PCMe material crystallization is not investigated yet.

In situ measurements of the resistivity temperature dependences are very sensitive method to crystallization transformations in the PCMe material layer, since the resistivities of the amorphous and crystalline phases differ by more than three orders of magnitude. The use of this method for the planar structures brings the experimental conditions closer to that of the real process and allows to analyze the influence of the neighboring conducting layers on the crystallization of the PCMe material film. Comparison of the results obtained by this method with that of the differential scanning calorimetry can give additional information about the peculiarities of the crystallization process in PCMe thin films.

So, the aim of this work was investigation of the influence of neighboring conducting layers on the crystallization kinetics and mechanism of $Ge_2Sb_2Te_5$ thin films using non-isothermal experiments by differential scanning calorimetry and in situ measurements of the resistivity temperature dependences.

Experimental

Thin films of the $Ge_2Sb_2Te_5$ composition were prepared at room temperature by dc magnetron sputtering of the stoichiometric polycrystalline target. The base pressure was 3.0×10^{-3} Pa, and the pressure of Ar during the process was 5.7×10^{-1} Pa. The dc power was 25 W, and the deposition rate was 4 Å s^{-1}. The thicknesses of $Ge_2Sb_2Te_5$ thin films were controlled by the atomic force microscopy (NT-MDT Solver Pro).

Elemental composition of the films was evaluated using the Auger spectroscopy (PerkinElmer PHI-660). The results showed that the composition of the deposited thin films was close to that of $Ge_2Sb_2Te_5$ and has a uniform distribution across the film thickness (Fig. 1).

X-ray diffraction data (Rigaku Smart Lab, step $\Delta\theta = 0.001°$, scanning speed 1° per minute, λ ($CuK_{\alpha1}$) = 1.5406 Å) showed that as-deposited films were amorphous (Fig. 2). Annealing at 200 °C for 30 min leads to the crystallization of as-deposited films. The crystalline structure of GST films annealed at 200 and 250 °C is identified as NaCl with space group Fm-3 m [36].

Thermal properties were investigated by differential scanning calorimetry (DSC-50, Shimadzu). For this purpose, GST225 films were deposited on c-Si substrates and had thicknesses of ~ 1 μm. Thin films were scraped from

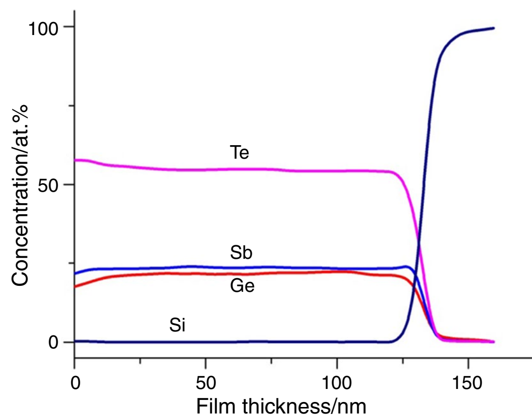

Fig. 1 Elemental distributions along the film thickness obtained by Auger spectroscopy

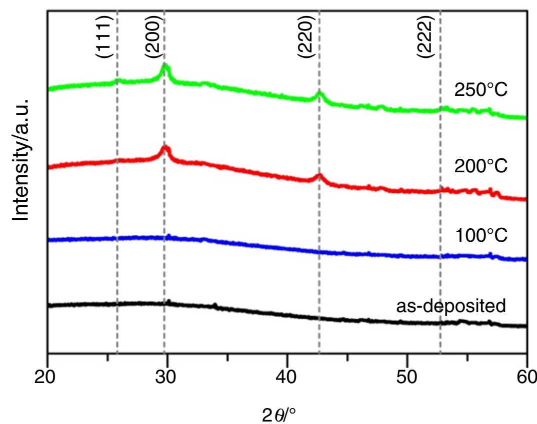

Fig. 2 Diffraction patterns of the as-deposited GST film and film after the heat treatment

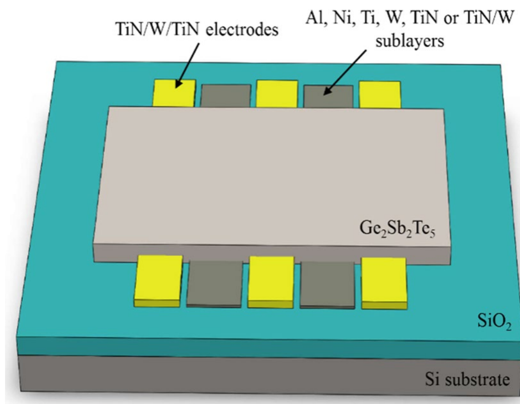

Fig. 3 The structure of the samples used in the experiments

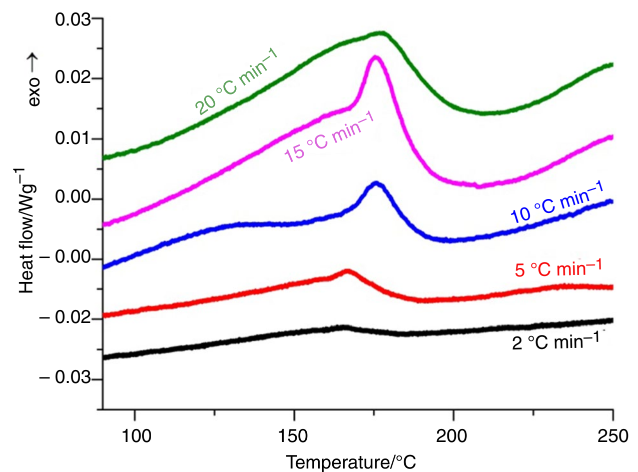

Fig. 4 DSC scans of GST225 thin films

the wafers with a sapphire spatula. Dispersity of the powder was estimated by the optical microscopy and was in the range of 1–30 µm. The powder samples had masses of a few milligrams and were pressed in Al pans. Empty Al pans were used as references. Temperature calibration was checked with In, Sn, Pb, Cd and Zn for all used heating rates. Measurements were carried out at five different heating rates (2, 5, 10, 15 and 20 °C min^{-1}) in a nitrogen flow (20 mL min^{-1}).

To study the temperature dependences of the resistivity, planar structures with TiN/W/TiN (30/50/15 nm) electrodes were formed on an oxidized silicon substrate. The distance between the electrodes was 1.5 mm. Then, six different conducting sublayers (Al, Ni, Ti, W, TiN or TiN/W) between the electrodes were fabricated. For this purpose, sublayers were deposited through the mask using the dc magnetron sputtering and have thicknesses of 40 nm. At last, $Ge_2Sb_2Te_5$ thin films with the thicknesses of 130 nm were deposited upon such structures through the mask. Figure 3 shows the structure of the samples used in the experiments.

The temperature dependences of the resistivity for thin films were investigated on a special setup, containing heating stage HFS600E-PB4 Linkam and picoammeter Keithley 6485. The measurements were carried out using five different heating rates (2, 5, 10, 15 and 30 °C min^{-1}) in an argon atmosphere.

Results and discussion

DSC scans for GST225 thin films scraped from the substrates and pressed in Al pans are shown in Fig. 4. For these samples, exothermic peaks are observed with the maximums in the temperature ranging from 165 to 180 °C, which corresponds to the phase transition from an amorphous state to a metastable cubic structure of the NaCl type according to the X-ray diffraction data.

The onset (T_x) crystallization temperatures were determined by the intersection of two baselines before and after

Table 1 Determined T_x and E_{ac}

Method	Sublayer	Heating rate						E_{ac}/eV
		2/ °C min^{-1}	5/ °C min^{-1}	10/ °C min^{-1}	15/ °C min^{-1}	20/ °C min^{-1}	30/ °C min^{-1}	
DSC	–	159.2	161.2	164.9	169	172.1	–	–
Resistivity	Without sublayer	152.7	155.3	159.3	163.3	–	167.3	0.40
	Al	153.5	158.8	162.5	165.7	–	170.5	0.41
	Ni	153.6	159.7	161.8	165.5	–	168.7	0.41
	Ti	155.9	160.5	163.9	167.0	–	171.0	0.42
	W	153.1	157.6	160.9	165.6	–	170.5	0.41
	TiN	153.2	157.7	160.4	163.4	–	167.9	0.41
	TiN/W	154.3	155.7	159.4	162.7	–	167.1	0.41

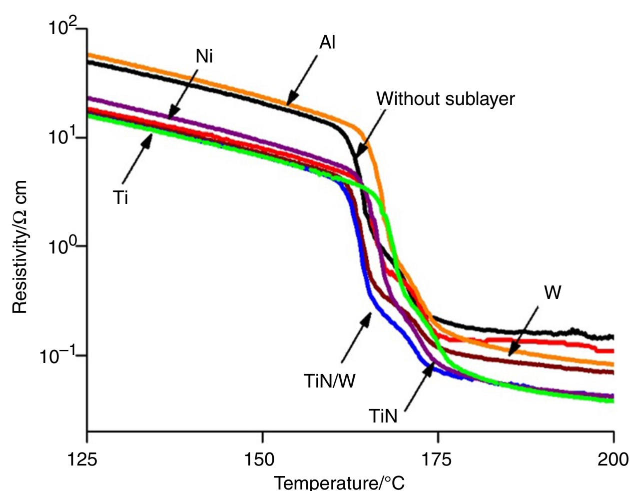

Fig. 5 The temperature dependences of the resistivity for GST225 thin films deposited on different sublayers

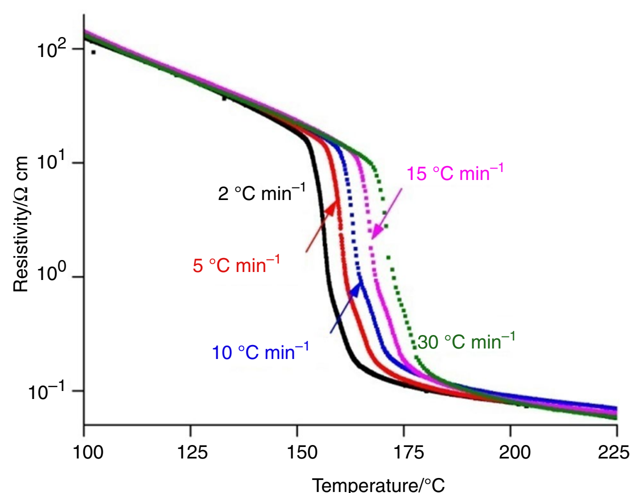

Fig. 6 The temperature dependences of the resistivity for GST225 thin films deposited on Al sublayer

the beginning of the exothermic peak due to the crystallization on the DSC curves (tangent method). The results of T_x determination are presented in Table 1.

Resistivity temperature dependences for GST225 thin films deposited on different sublayers for the heating rate 15 °C min^{-1} are shown in Fig. 5. Figure 6 presents resistivity temperature dependences for GST225 thin films deposited on the Al sublayer for different heating rates.

From the room temperature to 145 °C, exponential temperature dependences are observed indicating activation character of the conductivity of thin films in the amorphous state. In this case, the temperature dependences of the conductivities are described by the following expression [51]:

$$\sigma = \sigma_0 \exp\left(\frac{E_{ac}}{kT}\right), \tag{1}$$

where $_0$ is the pre-exponential factor, E_{ac} is the activation energy of the conductivity, and k is the Boltzmann constant.

Obtained activation energies of the conductivity (Table 1) are quite close ($E_{ac} = 0.41 \pm 0.01$ eV) for all investigated thin films and to the existing data [52, 53], which indicates the independence of the peculiarities of the conduction mechanism in GST225 amorphous films on the nature of adjacent layers.

When the temperature exceeds 145 °C, there appears sharp drop in resistivity by two orders of magnitude, which is due to the crystallization of the amorphous film. The crystallization temperatures were determined from the first derivative of the resistivity temperature dependences as the highest transition rate during crystallization [25, 32, 37–44] and are presented in Table 1.

As can be seen from Figs. 4, 6 and Table 1, T_x shifts to the higher temperatures with the increase in the heating rate indicating the retardation of the process and that the crystallization of the GST films proceeds in diffusive nucleation and growth mechanism [39].

Crystallization kinetics under isothermal conditions is described by the Johnson–Mehl–Avrami–Kolmogorov

model [54]. According to this model, the fraction of crystallites (conversion), α, can be written as:

$$\alpha = 1 - \exp\left(-k_r t^n\right), \tag{2}$$

where k_r is the reaction rate constant; t is the time; n is the kinetic (growth) exponent that is associated with the nucleation and growth mechanisms.

For thermally activated processes, the reaction rate constant is related with temperature by the Arrhenius equation:

$$k_r = A\exp\left(\frac{-E_a}{RT}\right), \tag{3}$$

where T is the temperature, E_a is the effective activation energy, A is the pre-exponential factor and R is the gas constant.

For the non-crystalline materials, transformation kinetics can be described by the following equation [55]:

$$\frac{d\alpha}{dt} = A\exp\left(\frac{-E_a}{RT}\right)f(\alpha), \tag{4}$$

where $f(\alpha)$ is the reaction model.

For non-isothermal conditions with constant heating rate $\beta = dT/dt$, as in our case, transformation kinetics can be described by the following equation:

$$\frac{d\alpha}{dT} = \frac{d\alpha}{dt}\frac{1}{\beta} = \frac{A}{\beta}\exp\left(\frac{-E_a}{RT}\right)f(\alpha) \tag{5}$$

where α is the fraction of crystallites (conversion), and $f(\alpha)$ is the reaction (crystallization) model.

Integral form of the reaction model $g(\alpha)$ can be obtained by integrating

$$g(\alpha) = \int_0^\alpha \frac{d\alpha}{f(\alpha)} = \frac{A}{\beta}\int_{T_0}^{T} \exp\left(\frac{-E_a}{RT}\right)dT = \frac{A}{\beta}I(E,T) = \frac{A}{\beta}\frac{E_a}{R}p(x), \tag{6}$$

where T_0 is the initial temperature; $I(E_a, T)$ is the temperature integral, which has no analytic solution; $p(x) = \int_0^\infty \left(e^{-x}/x^2\right)dx$, where $x = E_a/RT$, is the exponential integral, which can be found in mathematical tables.

Using these considerations, so-called kinetic triplet including effective activation energy, pre-exponential factor and reaction model $g(\alpha)$ can be found [56]. In this work, utilization of the different heating rates during the measurements of the resistivity temperature dependences and differential scanning calorimetry allowed us to estimate and compare crystallization kinetics of the GST225 films deposited on different sublayers using the isoconversional Ozawa–Flynn–Wall method [57–59]. Application of this method permitted to find effective activation energy and pre-exponential factor as a function of conversion.

For this purpose, the fraction of the crystallized material (conversion, α) must be calculated at first. For the experimental DSC curves, α was calculated assuming that the entire area of the phase transition peak corresponds to the fully passed reaction.

For the resistivity temperature dependency measurements, the conversion was calculated as follows [60]:

$$\alpha = \frac{\ln\sigma - \ln\sigma_a}{\ln\sigma_c - \ln\sigma_a}, \tag{7}$$

where σ_a and σ_c are the conductivity of the amorphous and crystalline phases, respectively, and σ is the conductivity of the partly crystallized thin film with the conversion α.

All temperature dependences of conversion calculated for DSC and resistivity measurements have S-shapes. Figure 7 presents temperature dependences determined from the resistivity temperature dependences for GST225 films deposited on the TiN sublayer.

Sigmoidal S-type shape of the temperature dependences of conversion is connected with the character of the process in solid state [61] indicating that crystallization of GST films is a complex process consisting of three stages. Evolution of the crystallization fraction α is slight enough at the beginning, increases rapidly at the second stage and finally slows down at the end. The initial stage corresponds to the induction period, when nucleation takes place. At this stage, appearing and dissociating nucleuses reach a critical size, after which probability of their growth became higher than dissociation. At the second stage, nucleuses begin to actively grow forming acceleration period. This stage is followed

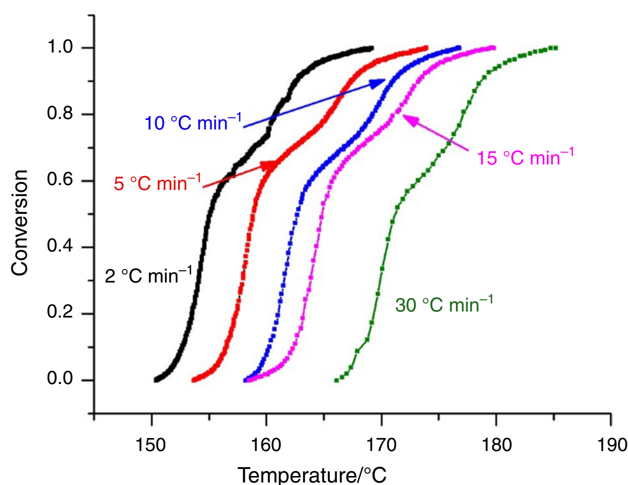

Fig. 7 Conversion temperature dependences determined from the resistivity temperature dependences for GST225 films deposited on the TiN sublayer

by the slowing crystallization rate, which happens when growing crystallites come into contact, begin to coalesce and form an ordered crystalline structure. However, distorted S-type shape of the conversion temperature dependences at the high values of α (nearby 0.6) can be due to the modification of crystallization mechanism.

The activation energy of crystallization (E_a) and pre-exponential factor (A) were derived from the slope and intercept, respectively, of the regression to the graph plotted using experimental data in the coordinates of Ozawa–Flynn–Wall method [57–59]. Figure 8 shows dependences of the effective activation energy on conversion obtained from the resistivity temperature dependences and DSC measurements.

We associate the difference between the dependences obtained by two measuring methods with the peculiarities of the sample preparation in these two methods. In the case of differential scanning calorimetry, the material is scraped from the substrate and pressed in the crucibles, thereby disrupting the continuity of the film, which leads to the appearance of multiple defects, which can play the role of nucleation centers and can promote crystallization. On the other hand, in the case of the resistivity measurements crystallization process depends on the properties of GST225 thin film and can be influenced by the neighboring sublayers. The certain difference in the effective activation energies of crystallization for the different sublayers confirms the influence of the neighboring conducting sublayers on the crystallization process. In addition, it was found that crystallization temperatures correlate with the effective activation energies and increase with the increase in E_a for GST225 thin films on different sublayers (Fig. 9), which also indicate this influence.

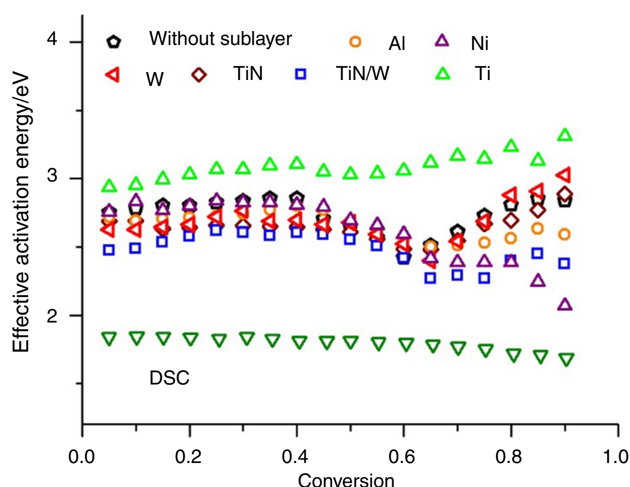

Fig. 8 Effective activation energy of the crystallization obtained by the measurements of the resistivity temperature dependences and differential scanning calorimetry

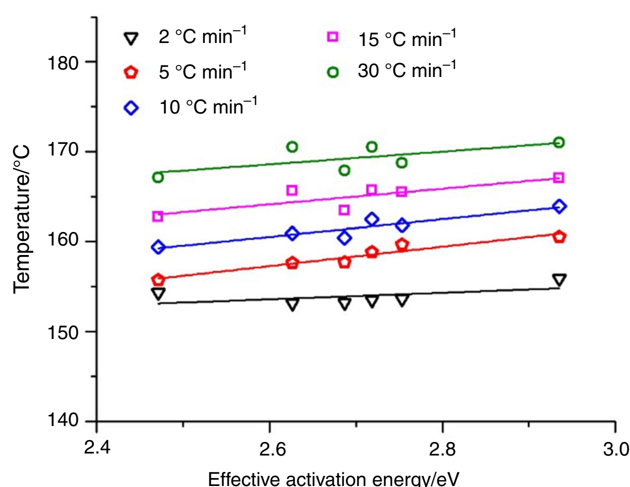

Fig. 9 Correlation between the crystallization temperatures and effective activation energies of the crystallization for GST225 thin films on different sublayers

So, obtained results indicate that crystallization process of amorphous GST225 thin films is affected by the conducting neighboring layers.

The highest effective activation energy of the crystallization is observed at the beginning of the crystallization process, which corresponds to the slowest initial period, and E_{ac} is nearly constant during this period. In most cases, effective activation energies slightly decrease in the range of conversion from 0.4 to 0.65, which is followed by the increase.

So, effective activation energy in the initial moment corresponds to the activation energy of nucleation rate E_{an}, while in the end—to the activation energy of crystalline growth rate E_{ag}. In the classical theory of nucleation and crystalline growth, the difference between the effective activation energies of the nucleation and crystalline growth rates corresponds to the energy barrier for the formation of nucleus with critical size $\Delta G^* = E_{an} - E_{ag}$. For the investigated GST225 thin films, this barrier is much less than 1 eV (Fig. 8). Such a low value indicates the sufficient role of the heterogeneous nucleation on the interfaces [22]. This conclusion explains found correlation between the crystallization temperatures and effective activation energies of the crystallization for GST225 thin films on different sublayers (Fig. 9).

In the work [62], mathematical model on the basis of the Kolmogorov–Johnson–Mehl–Avrami approach was developed for thin film crystallization process. According to this model, crystallization by means of the surface nucleation initially consists of both nucleation and growth, and since the surface is fully covered by the crystalline phase, the growth of previously emerged crystalline grains constitutes the ongoing crystallization. In this case, constant values of E_a (Fig. 8) correspond to the stage of nucleation and

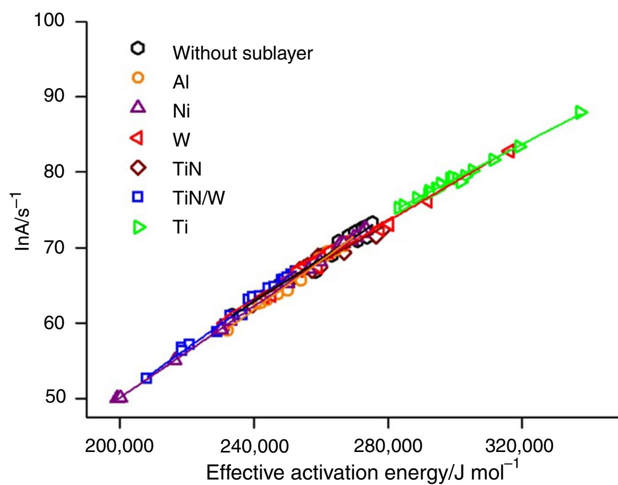

Fig. 10 Compensation effect for the investigated GST225 thin films

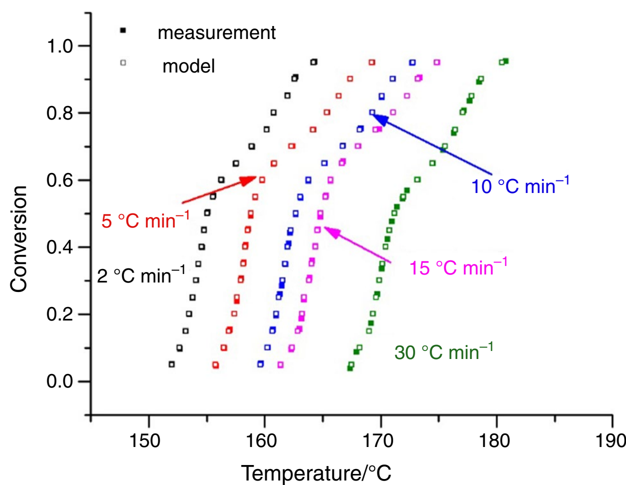

Fig. 11 Modeling of conversion temperature dependences for GST225 thin films on TiN sublayer

growth. Following decrease in E_a is connected with the growth of emerged crystalline grains, which gradually fill the film thickness. This stage influences the S-type shape of the conversion temperature dependences and leads to its distortion. The last range of increasing effective activation energies can be due to the coalescence of growing crystallites and formation of ordered crystalline structure.

Then, the compensation effect was used to determine the reaction model and pre-exponential factor (Fig. 10).

As can be seen from Fig. 11, pre-exponential factor A and effective activation energy are related by compensation effect [63]. In this case, the decrease in reaction rate due to the increase in the effective activation energy is compensated by the increase in the magnitude of ln$A$.

Then, Eq. (6) was used to calculate integral form of the reaction model $g(\alpha)$. The choice of the model was carried out from the best fitting of the calculated and plotted graph of the dependence of $g(\alpha)$ on conversion by theoretical reaction models. For this purpose, nineteen classical models were tested as theoretical reaction models [19], which can describe the processes in the solid phase. As a result, it was determined that the crystallization process in the investigated thin films is best described by the second- and third-order reactions. The reaction models found were confirmed using the model-fitting Coats–Redfern method [64].

Table 2 summarizes the parameters of the kinetic triplet (effective activation energy of crystallization E_a, pre-exponential factor A and reaction models $g(\alpha)$) obtained from the measurements of the resistivity temperature dependences and differential scanning calorimetry.

Determined kinetic triplets were used for modeling of conversion temperature dependences for all investigated sublayers and all heating rates. Figure 11 shows as example results of modeling for GST225 thin films on TiN sublayer.

As can be seen from Fig. 11, the obtained simulated dependences were close to the experimental results. Thus, the proposed method allows us to estimate the kinetic parameters with high accuracy.

Obtained kinetic triplets for the crystallization processes allow to determinate crystallization time for the investigated GST225 thin films and were used by us for the prediction of the possible data processing and storage

Table 2 Determined kinetic triplets obtained by two methods

Method	Sublayer	E_a/eV	ln$A$/s^{-1}	Reaction model
DSC	–	From 1.8 (α=0.05) to 1.7 (α=0.90)	From 45.9 (α=0.05) to 44.5 (α=0.90)	Second order
Resistivity	Without sublayer	From 2.8 (α=0.05) to 2.7 (α=0.95)	From 70.9 (α=0.05) to 66.8 (α=0.95)	Third order
	Al	From 2.7 (α=0.05) to 2.4 (α=0.95)	From 69.4 (α=0.05) to 58.9 (α=0.95)	Third order
	Ni	From 2.8 (α=0.05) to 2.4 (α=0.95)	From 70.4 (α=0.05) to 50.2 (α=0.95)	Third order
	Ti	From 2.9 (α=0.05) to 3.5 (α=0.95)	From 75.2 (α=0.05) to 87.9 (α=0.95)	Third order
	W	From 2.6 (α=0.05) to 3.3 (α=0.95)	From 67.2 (α=0.05) to 82.8 (α=0.95)	Third order
	TiN	From 2.7 (α=0.05) to 2.9 (α=0.95)	From 68.8 (α=0.05) to 71.5 (α=0.95)	Third order
	TiN/W	From 2.5 (α=0.05) to 2.2 (α=0.95)	From 63.1 (α=0.05) to 52.6 (α=0.95)	Third order

times of the PCMe cells. For this purpose, crystallization time was estimated by the equation [65]

$$t = \frac{g(\alpha)}{A\exp\left(\frac{E_\alpha}{RT}\right)}, \quad (8)$$

where $g(\alpha)$ is integral form of the found reaction model, and A is the pre-exponential factor.

In the works [66, 67], the parameter of failure time equal to 90% of the crystalline state ($\alpha = 0.9$) was estimated. We used obtained kinetic triplets to estimate crystallization times for investigated thin films with $\alpha = 0.9$, and comparison of these times with the data in the works [66, 67] is presented in Table 3.

As can be seen, the crystallization time published in the works [66, 67] for 110 °C is very different, which can be due to the different used methods, and indicates the problem of crystallization time estimation. It should be noted that crystallization times estimated in this work by DSC measurements are closer to the data in the work [66]. However, crystallization times estimated in this work by resistivity measurements are different for different adjacent layers confirming influence of neighboring layer on the crystallization process.

Next, crystallization times of the GST225 layers with different adjacent layers were estimated for the degree of conversion at which the conductivity of the GST225 film changed by one order of magnitude. Such a change in the conductivity is sufficient to distinguish and fix the logical states "0" and "1." A change in conductivity by one order of magnitude, for all studied materials of the sublayers, was recorded at various values of the degrees of conversion α. So, for GST225 films deposited on an oxidized silicon substrate, the α value was 0.45 for the Al and Ti sublayers, 0.50 for Ni, W and TiN and 0.55 for TiN/W. As a result, for the found values of the conversion degrees corresponding to one order change in the conductivity of GST225 thin films, we plotted the temperature dependence of crystallization time for the studied GST225 layers deposited on an oxidized silicon substrate and on various conductive sublayers. Figure 12 presents dependences of the crystallization times on the crystallization temperatures for the investigated GST225 thin films.

As can be seen from the graphs in Fig. 12 for the phase-change memory cells based on $Ge_2Sb_2Te_5$ thin films, it is possible to achieve data processing times on the order of units of nanoseconds at the crystallization temperatures above 340–410 °C, which is comparable with the recording time of the RAM devices (~ 10 ns). The phase transition time at room temperature, which corresponds to the data storage time, was also estimated, and according to the calculated values, it exceeds one hundred years. It should be noted that crystallization time of the GST225 thin films, which were measured on the substrate, is several orders of magnitude higher at room temperature than for the scraped material. This means that the probability of spontaneous crystallization is extremely small. Also, films on substrates at high temperatures have a shorter crystallization time. This is due

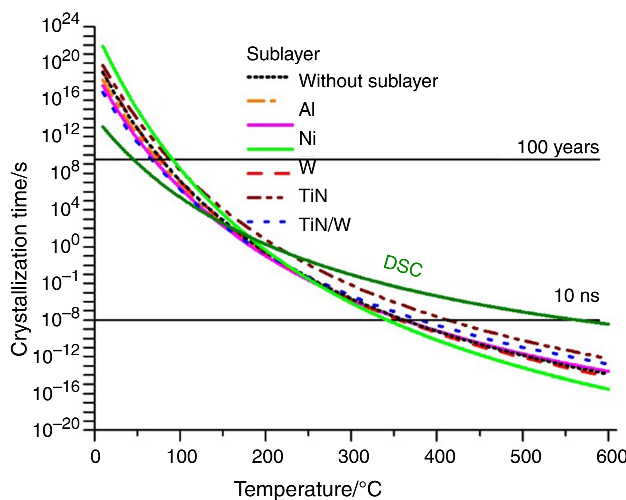

Fig. 12 Dependences of crystallization times on the crystallization temperatures for the investigated GST225 thin films

Table 3 Crystallization time according to the results of DSC and [66, 67]

Temperature, °C	Crystallization time/s								
	References	*This work*							
		DSC	*Resistivity*						
			Without sublayer	Al	Ni	Ti	W	TiN	TiN/W
50	7.1×10^{10} [66]	1.3×10^{13}	4.0×10^{13}	2.1×10^{15}	4.3×10^{20}	1.7×10^{14}	9.3×10^{11}	1.0×10^{12}	7.6×10^{14}
85	7.6×10^{6} [66]	2.3×10^{9}	2.8×10^{9}	1.9×10^{11}	4.8×10^{16}	3.1×10^{9}	5.7×10^{7}	9.0×10^{7}	1.3×10^{11}
110	9.1×10^{4} [66] 1.0×10^{7} [67]	5.4×10^{7}	8.5×10^{6}	7.2×10^{8}	2.0×10^{14}	4.3×10^{6}	1.7×10^{5}	3.2×10^{5}	7.3×10^{8}
125	8.5×10^{3} [66]	7.0×10^{6}	3.7×10^{5}	3.5×10^{7}	1.1×10^{13}	1.3×10^{5}	7.7×10^{3}	1.5×10^{4}	4.4×10^{7}

to the higher values of the effective activation energy. The higher effective activation energy at the beginning of the crystallization process leads to the higher stability of the amorphous state. In addition, the higher effective activation energy provides higher sensitivity of the crystallization process to the thermal effect, which explains higher crystallization rate of the GST225 layers on the substrates above ~ 150 °C than that estimated for the scraped thin films.

It should be noted that when the temperature reaches 340 °C, the crystallization time of the GST225 film on different sublayers can differ by more than three orders of magnitude. Thus, according to calculations, the fastest process can occur on the titanium sublayer (10 ns) and the slowest on the titanium nitride sublayer (1.9 µs). A GST225 thin film deposited on an oxidized silicon substrate without conductive sublayers has a crystallization time of ~ 65 ns, which is somewhat higher than on a titanium sublayer. Thus, to achieve a crystallization time of the order of 10 ns, the correct choice and strict control of the crystallization temperature of the GST225 layer are required depending on the sublayer used.

Conclusions

The influence of the adjacent layers (SiO_2, Al, Ni, Ti, W, TiN, TiN/W) on the crystallization kinetics of $Ge_2Sb_2Te_5$ thin films was investigated using the different techniques based on the application of two different methods—differential scanning calorimetry and measurements of the resistivity temperature dependences.

It was established that peculiarities of sample preparation sufficiently influence effective activation energy and pre-exponential factor. Effective activation energy of crystallization obtained by differential scanning calorimetry at the beginning of the crystallization was 1.8 eV and then slightly decreased to 1.7 eV at the end of the process. The values of the effective activation energy obtained from the measurements of the resistivity temperature dependences were in the range of 2.5–2.9 eV at the beginning and in the range of 2.2–3.5 eV at the end of the crystallization process. In the case of DSC, the material is scraped from the substrate and pressed in the crucibles, thereby disrupting the continuity of the film and leading to the appearance of multiple defects, which can play the role of nucleation centers and can promote crystallization. On the other hand, in the case of the resistivity measurements crystallization processes of GST225 thin films are influenced by the neighboring layers. The difference in the effective activation energies of crystallization for the GST225 thin films deposited on the different sublayers is caused by the influence of the neighboring sublayers on the crystallization process. It was found that crystallization temperatures correlate with the effective activation energies and increase with their growth.

The possible data processing and storage times of PCMe cells were determined. It was revealed that in the case of continuous film, not scraped from the substrate, the data storage time is higher, while data processing time is lower, which is due to the higher effective activation energy.

Acknowledgements This work was supported by Russian Science Foundation (Project Number 18-79-10231). The studies were performed using equipment of Core Facilities Center "MEMS and electronic components" and "STI Sensory" of MIET.

References

1. Kim JH, Byeon DS, Ko DH, Park JH. Physical and electrical characteristics of Ge_xSb_{100-x} films for use as phase-change materials. Thin Solid Films. 2018;659:1–6.
2. Sherchenkov A, Kozyukhin S, Babich A, Lazarenko P. Thermal properties of phase change material $Ge_2Sb_2Te_5$ doped with Bi. J Non-Cryst Sol. 2013;377:26–9.
3. Burr GW, Breitwisch MJ, Franceschini M, Garetto D, Gopalakrishnan K, Jackson B, Kurdi B, Lam C, Lastras LA, Padilla A, Rajendran B, Raoux S, Shenoy RS. Phase change memory technology. J Vac Sci Technol, B. 2010;28:223–62.
4. Zheng Q, Wang Y, Zhu J. Nanoscale phase-change materials and devices. J Phys D Appl Phys. 2017;50:243002.
5. Wang L, Ren W, Wen J, Xiong B. Overview of phase-change electrical probe memory. Nanomaterials. 2018;8:772.
6. Burr GW, Brightsky MJ, Sebastian A, Cheng HY, Wu JY, Kim S, Sosa NE, Papandreou N, Lung HL, Pozidis H, Eleftheriou E, Lam CH. Recent progress in phase-change memory technology. IEEE J Emerg Selected Topics Circuits Syst. 2016;6(2):146–62.
7. Guo P, Sarangan AM, Agha I. A review of germanium-antimony-telluride phase change materials for non-volatile memories and optical modulators. Appl Sci. 2019;9:530.
8. Raoux S, Wełnic W, Ielmini D. Phase change materials and their application to nonvolatile memories. Chem Rev. 2010;110:240–67.
9. Yamada N, Ohno E, Akahira N, Nishiuchi K, Nagata K, Takao MJ. High speed overwritable phase change optical disk material. J Appl Phys. 1987;26:61.
10. Redaelli A. Self-consistent numerical model. In: Phase change memory 2018 (pp. 65–88). Springer, Cham.
11. Athmanathan A, Stanisavljevic M, Papandreou N, Pozidis H, Eleftheriou E. Multilevel-cell phase-change memory: a viable technology. IEEE J Emerg Selected Topics Circuits Syst. 2016;6(1):87–100.
12. Skelton JM, Loke D, Lee TH, Elliott SR. Understanding the multistate SET process in Ge–Sb–Te–based phase-change memory. J Appl Phys. 2012;112:064901.
13. He Q, Li Z, Peng JH, Deng YF, Zeng BJ, Zhou W, Miao XS. Continuous controllable amorphization ratio of nanoscale phase change memory cells. Appl Phys Lett. 2014;104:223502.
14. Yang F, Xu L, Chen J, Xu J, Yu Y, Ma Z, Chen K. Nanoscale multilevel switching in $Ge_2Sb_2Te_5$ thin film with conductive atomic force microscopy. Nanotechnology. 2015;27(3):035706.
15. Yamada N, Ohno E, Nishiuchi K, Akahira N, Takao M. Rapid-phase transitions of GeTe–Sb2Te3 pseudobinary amorphous thin films for an optical disk memory. J Appl Phys. 1991;69(5):2849–56.

16. Jeong TH, Kim MR, Seo H, Kim SJ, Kim SY. Crystallization behavior of sputter-deposited amorphous $Ge_2Sb_2Te_5$ thin films. J Appl Phys. 1999;86:774–8.
17. Park J, Kim MR, Choi WS, Seo H, Yeon C. Characterization of amorphous phases of $Ge_2Sb_2Te_5$ phase-change optical recording material on their crystallization behavior. Jpn J Appl Phys. 1999;38:4775–9.
18. Seo H, Jeong TH, Park JW, Yeon C, Kim SJ, Kim SY. Investigation of crystallization behavior of sputter-deposited nitrogen-doped amorphous $Ge_2Sb_2Te_5$ thin films. Jpn J App. Phys. 2000;39:745–51.
19. Sherchenkov A, Kozyukhin S, Babich A. Estimation of kinetic parameters for the phase change memory materials by DSC measurements. J Therm Anal Calorim. 2014;117(3):1509–16.
20. Svoboda R, Karabyn V, Malek J, Frumar M, Benes L, Vlcek M. Amorphous-to-crystalline transition in $Ge_8Sb_{(2-x)}Bi_xTe_{11}$ phase-change materials for data recording. J Alloys Compd. 2016;674:63–72.
21. Karabyn V, Himics D, Prikryl J, Benes L, Svoboda R, Frumarova B, Wagner T, Frumar M. Physico-chemical properties of the $Ge_8Sb_{2-x}Bi_xTe_{11}$ bulks and thin films. Chalcogenide Lett. 2017;14(11):489–97.
22. Aly KA. Crystallization study of $Se_{86}Sb_{14}$ glass. J Therm Anal Calorim. 2017;129:709–14.
23. Babich A, Sherchenkov A, Kozyukhin S, Lazarenko P, Boytsova O, Shuliatyev A. Effect of doping on the crystallization kinetics of phase change memory materials on the basis of Ge–Sb–Te system. J Therm Anal Calorim. 2017;127(1):283–90.
24. Kato N, Konomi I, Seno Y, Motohiro T. In situ X-ray diffraction study of crystallization process of GeSbTe thin films during heat treatment. Appl Surf Sci. 2015;244:281–4.
25. Ruitenberg G, Petford-Long AK, Doole RC. Determination of the isothermal nucleation and growth parameters for the crystallization of thin $Ge_2Sb_2Te_5$ films. J Appl Phys. 2002;92(6):3116–23.
26. Privitera S, Bongiorno C, Rimini E, Zonca R. Crystal nucleation and growth processes in $Ge_2Sb_2Te_5$. Appl Phys Lett. 2004;84(22):4448–50.
27. Pandian R, Kooi BJ, De Hosson JTM, Pauza A. Influence of capping layers on the crystallization of doped Sb_xTe fast-growth phase-change films. J Appl Phys. 2006;100(12):123511.
28. Privitera S, Lombardo S, Bongiorno C, Rimini E, Pirovano A. Phase change mechanisms in $Ge_2Sb_2Te_5$. J App Phys. 2007;102(1):013516.
29. Ohshima N. Crystallization of germanium–antimony–tellurium amorphous thin film sandwiched between various dielectric protective films. J Appl Phys. 1996;79(11):8357–63.
30. Tominaga J, Nakano T, Atoda N. Double optical phase transition of GeSbTe thin films sandwiched between two SiN layers. Jpn J Appl Phys. 1998;37(1):1852–4.
31. Men L, Tominaga J, Fuji H, Kikukawa T, Atoda N. The effects of metal-doped GeSbTe films on light scattering-mode super-resolution near-field structure (super-RENS). Jpn J Appl Phys. 2001;40(1):1629–33.
32. Weidenhof V, Friedrich I, Ziegler S, Wuttig M. Laser induced crystallization of amorphous $Ge_2Sb_2Te_5$ films. J Appl Phys. 2001;89(6):3168–76.
33. Kim D, Kim SJ, An SH, Kim SY. Ellipsometric simulation and preliminary observation of fast crystallization behavior of $Ge_2Sb_2Te_5$ amorphous thin films at elevated temperature. Jpn J Appl Phys. 2003;42(8):5107–12.
34. Morales-Sanchez E, Prokhorov EF, Gonzalez-Hernandez J, Mendoza-Galvan A. Structural, electric and kinetic parameters of ternary alloys of GeSbTe. Thin Solid Films. 2005;471(1–2):243–7.
35. Rodríguez CVR, Sanchez EM, Hernández JG, Prokhorov E, Saldaña JM, Martínez GT. Estimate of the crystallization kinetics in stoichiometry compositions films of Ge:Sb:Te. J Surf Eng Mater Adv Technol. 2012;2(1):44–6.
36. Friedrich I, Weidenhof V, Njoroge W, Franz P, Wuttig M. Structural transformations of Ge2Sb2Te5 films studied by electrical resistance measurements. J Appl Phys. 2000;87(9):4130.
37. González-Hernández J, Prokhorov E, Vorobiev Y. Temperature dependence of structure and electrical properties of germanium-antimony-tellurium thin film. J Vac Sci Technol A Vacuum Surf Films. 2000;18(4):1694–700.
38. Wamwangi D, Njoroge WK, Wuttig M. Crystallization kinetics of $Ge_4Sb_1Te_5$ films. Thin Solid Films. 2002;408(1–2):310–5.
39. Privitera S, Rimini E, Bongiorno C, Zonca R, Pirovano A, Bez R. Crystallization and phase separation in $Ge_{2+x}Sb_2Te_5$ thin films. J Appl Phys. 2003;94(7):4409–13.
40. Njoroge WK, Dieker H, Wuttig M. Influence of dielectric capping layers on the crystallization kinetics of $Ag_5In_6Sb_{59}Te_{30}$ films. J Appl Phys. 2004;96(5):2624–7.
41. Wei X, Shi L, Chong TC, Zhao R, Lee HK. Thickness dependent nano-crystallization in $Ge_2Sb_2Te_5$films and its effect on devices. Jpn J Appl Phys. 2007;46(1):2211–4.
42. Cheng HY, Kao KF, Lee CM, Chin TS. Crystallization kinetics of Ga–Sb–Te films for phase change memory. Thin Solid Films. 2008;516(16):5513–7.
43. Choi Y, Jung M, Lee YK. Effect of heating rate on the activation energy for crystallization of amorphous $Ge_2Sb_2Te_5$ thin film. Electrochem Solid-State Lett. 2009;12(7):F17–9.
44. Huang YJ, Chen YC, Hsieh TE. Phase transition behaviors of Mo- and nitrogen-doped $Ge_2Sb_2Te_5$ thin films investigated by in situ electrical measurements. J Appl Phys. 2009;106(3):034916.
45. Huang YJ, Chung TC, Wang CH, Hsieh TE. Characterizations of AgInSbTe and its nanocomposite thin films for phase-change memory applications. J Electrochem Soc. 2010;157(12):P113–8.
46. Chang PC, Chang SC, Chin TS. Crystallization kinetics and X-ray photoelectron spectroscopy of Ga_2TeSb_7 thin film. J Vac Sci Technol. 2011;29(4):04D111.
47. Muchira IW, Njoroge WK, Karimi PM. Crystallization kinetics of In40Se60 thin films for phase change random access memory (PRAM) applications. J Ovonic Res. 2015;11(3):131–6.
48. Smili B, Abadlia L, Bouchelaghem W, Fazel N, Kaban I, Gasser F, Gasser JG. Crystallization kinetics study of melt-spun $Zr_{66.7}Ni_{33.3}$ amorphous alloy by electrical resistivity measurements. J Therm Anal Calorim. 2019;136(3):1053–67.
49. Sherchenkov A, Kozyukhin S, Babich A, Lazarenko P, Kalugin V, Timoshenkov S, Borgardt N, Sybina Y. Crystallization mechanism and kinetic parameters in $Ge_2Sb_2Te_5$ thin films for the phase change memory application. Chalcogenide Lett. 2018;15(1):45–54.
50. Miyagawa N. Overview of blu-ray disc™ recordable/rewritable media technology. Front Optoelectron. 2014;7(4):409–24.
51. Mott NF, Davis EA. Electronic processes in non-crystalline materials. 2nd ed. Oxford: Oxford University Press; 1979.
52. Kato T, Tanaka K. Electronic properties of amorphous and crystalline $Ge_2Sb_2Te_5$ films. Jpn J Appl Phys. 2005;44(10):7340–4.
53. Xu L, Tong L, Geng L, Yang F, Xu J, Su W, Liu D, Ma Z, Chen K. A comparative study on electrical transport properties of thin films of $Ge_1Sb_2Te_4$ and $Ge_2Sb_2Te_5$ phase-change materials. J Appl Phys. 2011;110(1):013703.
54. El-Oyoun MA. An investigation of the kinetic transformation mechanism of $Ge_{12.5}Te_{87.5}$ chalcogenide glass under non-isothermal regime. J Non Cryst Solids. 2011;357(7):1729–35.
55. Vyazovkin S. Modification of the integral isoconversional method to account for variation in the activation energy. J Comput Chem. 2001;22(2):178–83.
56. Vyazovkin S, Burnham AK, Criado JM, Pérez-Maqueda LA, Popescu C, Sbirrazzuoli N. ICTAC Kinetics Committee

recommendations for performing kinetic computations on thermal analysis data. Thermochim Acta. 2011;520(1–2):1–19.
57. Mothé CG, de Freitas JS. Lifetime prediction and kinetic parameters of thermal decomposition of cashew gum by thermal analysis. J Therm Anal Calorim. 2018;131:397–404.
58. Aboulkas A, El Harfi K. Study of the kinetics and mechanisms of thermal decomposition of Moroccan Tarfaya oil shale and its kerogen. Oil Shale. 2008;25(4):426–43.
59. Kongkaew N, Pruksakit W, Patumsawad S. Thermogravimetric kinetic analysis of the pyrolysis of rice straw. Energy Procedia. 2015;79:663–70.
60. Mehta N, Kumar A. Studies of crystallization kinetics in a-$Se_{80-x}Te_{20}Cd_x$ and a-$Se_{80-x}Te_{20}Ge_x$ alloys using D.C. conductivity measurements. J Therm Anal Calorim. 2006;83(3):669–73.
61. Barre P. Kinetika geterogennih processov (in Russian). Moscow: Mir Publishers; 1976.
62. Vorobyov V, Lazarenko P, Sherchenkov A, Vishnyakov N, Ermachikhin A, Kozyukhin S. Kinetics of volume and surface driven crystallization in thin films. J Phys: Condens Matter. 2020;32:355401.
63. Krongauz VV, Bennett SE, Ling MTK. Kinetics of water vapor diffusion in resins. J Therm Anal Calorim. 2016;125(1):231–43.
64. Ganeshan G, Shadangi KP, Mohanty K. Degradation kinetic study of pyrolysis and co-pyrolysis of biomass with polyethylene terephthalate (PET) using Coats-Redfern method. J Therm Anal Calorim. 2018;131(2):1803–16.
65. Brown M. Handbook of thermal analysis and calorimetry. Amsterdam: Elsiever Science B.V; 1998.
66. Sutou Y, Kamada T, Sumiya M, Saito Y, Koike J. Crystallization process and thermal stability of Ge1Cu2Te3 amorphous thin films for use as phase change materials. Acta Mater. 2012;60(3):872–80.
67. Zhang T, Song Z, Wang F, Liu B, Feng S, Chen B. Te-free SiSb phase change material for high data retention phase change memory application. Jpn J Appl Phys. 2017;46(7L):L602–4.

Publisher's Note Springer Nature remains neutral with regard to jurisdictional claims in published maps and institutional affiliations.